Article | Received 27 January 2024; Accepted 23 April 2024; Published 26 April 2024
https://doi.org/10.55092/sc20240003

Computer vision-based displacement identification and its application to bridge condition assessment under operational conditions

Zhen Peng [1], Jun Li [1,*], Hong Hao [1,2]

[1] Centre for Infrastructural Monitoring and Protection, School of Civil and Mechanical Engineering, Curtin University, WA 6102, Australia

[2] Earthquake Engineering Research and Test Center, Guangzhou University, Guangzhou, China

* Correspondence author; Email: junli@curtin.edu.au.

Abstract: Bridge damage detection is crucial for ensuring the safety and integrity of the bridge structure. Traditional methods for damage detection often rely on manual inspections or sensor-based measurements, which can be time-consuming and costly. In recent years, computer vision techniques have shown promise in bridge displacement measurement and damage detection. The objective of this study is to extract reliable features from displacement measured with computer vision-based method that are sensitive to structural condition change while robust to the variation of operational condition. In particular, this research paper presents a novel approach for bridge damage detection using an indicator defined based on the transverse influence ratio (DTIR) from computer vision-based displacement measurements. The proposed method utilizes computer vision algorithms to extract bridge girder displacement responses under moving load. The DTIR indicator, defined as the vehicle-induced bridge quasi-static displacement ratio between two adjacent girders, is extracted as the damage-sensitive feature. Theoretical derivation proves that DTIR indicator is only related to the structural condition and the transverse position of a vehicle over the deck, while independent of the variation of vehicle weight and speed. To validate the effectiveness of the proposed method, a series of drive-by experiments were performed on a multi-girder beam bridge with different structural conditions. The results demonstrated the capability of the proposed approach in accurately detecting the occurrence and possible location of structural damage. Furthermore, the paper discusses the advantages and limitations of the DTIR indicator for bridge damage detection, as well as how to generalize the proposed method to bridges with more than two traffic lanes. In conclusion, the proposed method offers a promising solution for low cost, easy deployable and scalable health monitoring solution for bridges under operating conditions.

Keywords: computer vision; bridge condition assessment; damage detection; operational condition

1. Introduction

Civil structures surely deteriorate under normal operating conditions owing to fatigue and corrosion, and may suffer various levels of damage under extreme conditions, such as earthquake, typhoon, wave and accidental impact. The accumulation of structural deterioration will adversely affect the serviceability, integrity, reliability and shorten the service life of civil engineering structures. Structural health monitoring (SHM) and condition assessment are crucial for ensuring safety, reducing life-cycle maintenance costs and preserving the service life of existing infrastructure [1–3]. Given the limited budget allocated to infrastructure maintenance, it is desirable to develop cost-effective, easy deployable and scalable SHM techniques that are applicable to a larger population of infrastructures under normal operation conditions to avoid or minimize interruption of structural functions [4–6].

In the last decades, computer vision-based SHM techniques have been extensively developed and applied in the structural local level surface crack detection [7], bolt loose detection [8] and displacement responses measurements. The measured displacement responses can be further used in global level structural system identification [9], bridge vibration serviceability evaluation [10], model updating [11] and damage detection [12]. The displacement response under traffic load is usually selected as a critical parameter for evaluating bridge performance. However, conventional contact-type displacement sensors such as the linear variable differential transducer (LVDT) require a stationary reference point, which is often difficult to find in the field. Furthermore, the measurement range of traditional displacement sensor is relatively short, which limit its application to large-span bridge structures. Thanks to the rapid advances in computer vision, the camera-based noncontact vision sensing has emerged as a promising alternative to conventional contact sensors for structural dynamic displacement and strain distribution measurement. Significant advantages of the vision sensor include its low cost, ease of setup and operation, and flexibility to extract displacements of any points on the structure from a single video measurement. Therefore, the scope of this work falls in extracting reliable damage sensitive features from displacement responses of bridge structure under traffic load. Although the research community has recently made significant progress in estimating the 2D and 3D pixel or sub-pixel level structural displacement responses using computer vision-based techniques, how to convert the massively available data extracted by computer vision-based methods into more actionable information that can aid the high lever decision-making is still an open area of research [13]. To achieve the goal of effective and accurate SHM and condition assessment, extracting reliable damage sensitive feature from computer vision-based displacement data is highly demanded. In this regard, structural modal parameters, *i.e.* natural frequency, mode shape and damping ratio have long been used as damage features. In conventional vibration test, the spatial resolution of the obtained mode shape is limited by the number of vibration sensors deployed along the structure. Furthermore, the attached sensors may vary the structural mass matrix and bias the identified mode shape when the structure is lightweight.

On the contrary, the video camera is contactless and simultaneously obtains multi-points or even full-field displacement mode shape [14–16]. The modal parameters identified from vision-based technique can be further used to update finite element (FE) model by comparing the analytical and experimental modal information [17].

For bridge structures subjected to traffic load, the dynamic displacement responses mainly consist of a low-frequency quasi-static component and a relatively high-frequency modal vibration component. In theory, the displacement can be reconstructed from acceleration responses via double integration. Therefore, the transfer function between acceleration and displacement in the frequency domain is $FFT(u,\omega)/FFT(a,\omega) = -1/\omega^2$, where ω represents circular frequency. The transfer function indicates that the high-frequency displacement component is weak, and the quasi-static component in the low-frequency region mainly dominates the energy of bridge displacement responses. This property makes it difficult to obtain the bridge parameters of high modes from displacement responses of a bridge under moving load. However, they can be conveniently identified from acceleration responses. As a result, most of the vision-based bridge modal identification methods are conducted in a controlled laboratory environment with artificially generated external excitation, while little research has been found on in-situ bridges subjected to normal operational load. Even in such cases, only the low-order mode shape can be identified. Instead, it is appropriate to extract reliable features from the bridge quasi-static displacement component for model updating and damage detection. In this regard, the bridge displacement influence line is a desirable quasi-static feature that has a strict relationship with the structural flexibility matrix and can thus serve as a damage-sensitive feature [18]. In Reference [19], the computer vision technique is employed to simultaneously identify the vehicle location information and bridge displacement responses. Experiment and field verification results prove that the bridge displacement influence line can be identified from the information obtained from a video camera. In Reference [11], the computer vision-based displacement identification, along with the vehicle axle load, is used to identify the bridge influence line at different target positions. The identified influence line is further used to update the FE model. In Reference [9,20], the bridge displacement influence surface is identified using computer vision-based techniques. A damage indicator is developed from the bridge displacement influence surface to detect the presence and location of bridge structural damage.

Existing research works have demonstrated that the bridge displacement influence line/surface identified from computer vision techniques are promising in bridge model updating and damage detection. However, it is noted that the corresponding vehicle axle load, along with the vehicle location information, should be known in advance. This limitation restricts the practical use of vision-based influence line/surface as a damage-sensitive feature for bridge condition assessment in a few cases. Typically, the vehicle location on the bridge can be obtained from traffic survey cameras installed above the bridge deck. The vehicle axle load is usually measured by the weigh-in-motion (WIM) system, which significantly increases the overall structural health monitoring (SHM) implementation costs. To address the aforementioned limitation of the displacement influence line-based damage detection method, this paper aims to develop a cost-effective, easily deployable, and scalable bridge

SHM approach using vision-based measurements. Specifically, a reliable damage-sensitive feature will be extracted from bridge displacement measured with the computer vision-based method in a fully data-driven manner, eliminating the need for any information regarding the traffic conditions.

The remainder of this paper is organized as follows. Section 2 introduces the theoretical basis of the displacement transverse influence ratio (DTIR). Section 3 provides the procedures of the proposed method, including computer vision-based bridge displacement identification, quasi-static displacement component extraction, peak value detection, and DTIR indicator estimation. Section 4 presents the details of the experimental setup, damage scenarios, and damage detection results. Finally, the conclusion is provided in Section 5.

2. Theoretical derivation of DTIR

This section will revisit the concept of the bridge influence surface, which provides the theoretical basis for the proposed damage feature extraction method. The two-dimensional bridge influence surface is an extension of the well-known one-dimensional influence line. Specifically, the influence surface at a certain measurement location on the bridge is defined as the response function of the unit load with respect to any location on the structure. An illustration of the moving vehicle load applied on the bridge deck and the corresponding bridge influence surface concept is presented in Figure 1.

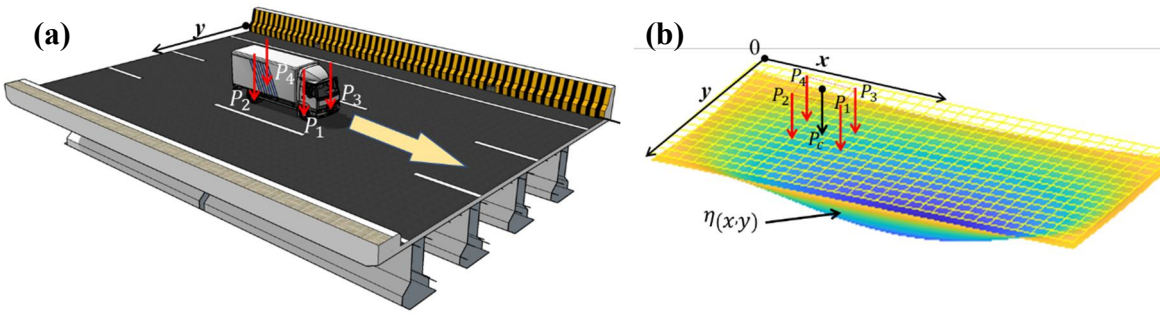

Figure 1. (a) Moving vehicle load applied on bridge deck, **(b)** illustration of bridge influence surface.

Under the linear-elastic assumption, the influence surface can be employed to calculate the quasi-static displacement responses of the bridge at the measurement location $(\bar{x}_a, \bar{y}_a)$ on a bridge girder induced by a set of moving wheel loads $\{P_1, P_2, \dots, P_k\}$

$$u(\bar{x}_a, \bar{y}_a) = \sum_{i=1}^{k} \emptyset_{daf} \cdot \eta_{\bar{x}_a, \bar{y}_a}(x_i, y_i) \cdot P_i(x_i, y_i) \tag{1}$$

where $\emptyset_{daf}$ denotes the dynamic amplification factor due to the bridge-vehicle interaction effect. In this study, a low-pass filter will be applied to the vision-based displacement to discard the dynamic part of the raw data while preserving the static response. Therefore, the bridge-vehicle interaction effect can be neglected. P_i denotes the i-th wheels load applied at location (x_i, y_i). $\eta_{\bar{x}_a, \bar{y}_a}(x_i, y_i)$ is the displacement influence surface

coefficient under vehicle loading. It is noted that $\eta_{\bar{x}_a,\bar{y}_a}(x_i, y_i)$ is a function of structural condition and load location (x_i, y_i), while independent of the wheels load weight. Under the linear-elastic assumption, the influence surface $\eta_{\bar{x}_a,\bar{y}_a}(x_i, y_i)$ can be approximated by the product of longitudinal influence line and transverse influence line, namely

$$\eta_{\bar{x}_a,\bar{y}_a}(x_i, y_i) = \eta_{\bar{x}_a}(x_i) \cdot \eta_{\bar{y}_a}(y_i) \tag{2}$$

Equation (1) can be simplified by replacing the set of moving wheels loads $\{P_1, P_2, \ldots, P_k\}$ with an equivalent concentrated load P_c applied at the vehicle centroid (x_c, y_c).

$$u(\bar{x}_a, \bar{y}_a) = \eta_{\bar{x}_a}(x_c) \cdot \eta_{\bar{y}_a}(y_c) \cdot P_c(x_c, y_c) \tag{3}$$

The bridge influence line/surface can be identified from Equation (2) when the vehicle loading information and bridge displacement responses at a certain location are available [21]. Thanks to the rapid advances in computer vision, it is now possible to conveniently identify in-situ bridge displacement responses subjected to traffic load at a low cost [22,23]. However, in practical SHM implementation, the vehicle load P_c along with the vehicle trajectory information are usually expensive to measure and difficult to synchronize with bridge displacement responses. Therefore, when only the bridge displacement response is available, it is desirable to develop a data-driven damage sensitive feature independent of the vehicle load. Inspired by the authors' previous work on normalizing traffic-induced bridge cable force [24], this study attempts to normalize the effects of vehicle loading by introducing displacement responses of two points at the same longitudinal and different transverse locations.

Similar to Equation (2), the quasi-static displacement responses at bridge location $(\bar{x}_a, \bar{y}_b)$ subjected to the same vehicle load can be written as

$$u(\bar{x}_a, \bar{y}_b) = \eta_{\bar{x}_a}(x_c) \cdot \eta_{\bar{y}_b}(y_c) \cdot P_c(x_c, y_c) \tag{4}$$

It should be noted that the longitudinal location x_c varies with time as the vehicle passes the bridge. However, the longitudinal influence line coefficient $\eta_{\bar{x}_a}(x_c)$ appearing in Equation (3) and Equation (4) remains the same since the relative longitudinal distance between the two displacement measurement points and the vehicle is identical. The DTIR indicator between the two measurement points $(\bar{x}_a, \bar{y}_a)$ and $(\bar{x}_a, \bar{y}_b)$ can be calculated as

$$DTIR_{\bar{y}_a,\bar{y}_b} = \frac{u(\bar{x}_a, \bar{y}_a)}{u(\bar{x}_a, \bar{y}_b)} = \frac{\eta_{\bar{x}_a}(x_c) \cdot \eta_{\bar{y}_a}(y_c) \cdot P_c(x_c, y_c)}{\eta_{\bar{x}_a}(x_c) \cdot \eta_{\bar{y}_b}(y_c) \cdot P_c(x_c, y_c)} = \frac{\eta_{\bar{y}_a}(y_c)}{\eta_{\bar{y}_b}(y_c)} \tag{5}$$

It is seen from Equation (5) that the transverse displacement influence ratio is related to the structural condition and the vehicle location y_c in transverse direction over the bridge deck, while independent of the weight and the longitudinal location of vehicle. For a bridge structure carries single traffic lane, the equivalent concentrated vehicle transverse location y_c corresponding to each vehicle trip will be approximately equal, thus, $DTIR_{\bar{y}_a,\bar{y}_b}$ defined in Equation (5) can directly server as damage feature. For a bridge structure carries multi-traffic lane, the equivalent concentrated vehicle transverse location y_c will be different when the vehicle presents on different traffic lane. Consequently, $DTIR_{\bar{y}_a,\bar{y}_b}$ corresponding to a population of vehicle trips will statistically form a multi-cluster feature space. The number

of clusters in the feature space will be the same to the number of traffic lane. The proposed method is data-driven, without a finite element (FE) model; therefore, it's difficult to quantitatively suggest a universal threshold of $DTIR$ that is applicable to different bridges. However, from long-term SHM perspectives, the mean value and 95% confidence interval of $DTIR$ can be periodically checked for changes. In field application, if the $DTIR$ of a specific girder consistently lies outside the 95% interval, the bridge owner can organize a field inspection for this girder. A more detailed analysis of the variation of DTIR with changes in structural condition will be provided in Section 4.

As mentioned before, the bridge influence line/surface is a function of the structural flexibility matrix, which changes when structural damage occurs. Considering that the vehicle generally remains within the lane lines, except for very few lane changes, the transverse displacement influence ratio can statistically serve as a robust damage-sensitive feature. In Equation (5), the displacement responses used to calculate the transverse displacement influence ratio are taken at the point in time when the peak value of displacement occurs. When the vehicle is approaching or leaving the bridge, the target displacement measurement points far away from the load has small displacement response. Consequently, the transverse displacement influence ratio estimated from vision-based displacement measurement at lower values is not reliable, especially when the camera is placed at a long distance from the target.

3. Estimation of DTIR indicator using computer vision

3.1. Computer vision-based bridge displacement measurements

The rapid advances in cameras and computer vision algorithms enable the accurate measurement of bridge displacement, offering several advantages over traditional sensors, including: i) unlike conventional contact-type displacement sensors, vision sensors do not require physical access to the structures; ii) the measurement range of traditional non-contact-type laser displacement sensors is relatively short, limiting their application to large-span bridge structures. However, cameras equipped with lenses can be set up at distances of dozens or even hundreds of meters from the structures.

In this study, a displacement tracking method based on the SIFT (Scale-Invariant Feature Transform) keypoint detector and the Fast Library for Approximate Nearest Neighbors (FLANN) based matcher was used to measure vehicle-induced bridge vertical displacement. Hereafter, this displacement tracking method is referred to as the SIFT-FLANN-based method, which has been included in the OpenCV library. It has been reported that the SIFT-FLANN-based method can estimate the displacement with desirable accuracy and efficiency [25]. The main steps of the computer vision-based displacement identification are given below:

Step 1: source video pre-processing and scale factor determination. In practical applications, the camera axis and lens may not be perpendicular to the motion plane of the measurement target. To address this issue, a homography transformation is adopted to establish a mapping between the image plane and the target plane. The homography transformation matrix **H** can be estimated with a minimum of 4 pairs of points on both planes [26]. The

homography transformation is a practical method for camera calibration and scale factor determination, suitable for in-plane motion and lenses without distortion [19]. Then, the scale factor between the actual dimension in physical units (e.g., mm) and the image dimension in pixels is calculated from the first frame.

Step 2: features detection and description in the ROI of the first frame. In the first frame, an ROI of the target structure with distinct corners and textures that stand out from the surrounding background is selected. Each feature point extracted from the SIFT algorithm consists of a feature detector and a descriptor. The feature detector stores the location and orientation of the feature point, while the descriptor contains information about the gradient magnitude and orientation within the region surrounding the keypoint.

Step 3: features matching and tracking in all subsequent frames. The feature points extracted from the subsequent frames are matched with the feature points in the first frame based on the similarity of the descriptors.

Step 4: Displacement conversion and post-processing. The displacement identification results are converted from subpixel values to physical displacements using the scale factor determined in Step 1. Interpolation is used to replace the very few NaN values for better resolution.

3.2. Quasi-static displacement component extraction

Bridge displacement response $u(t)$ induced by moving load consists of quasi-static component $u_s(t)$ and dynamic component $u_d(t)$, as shown in Figure 2.

$$u(t) = u_s(t) + u_d(t) \tag{6}$$

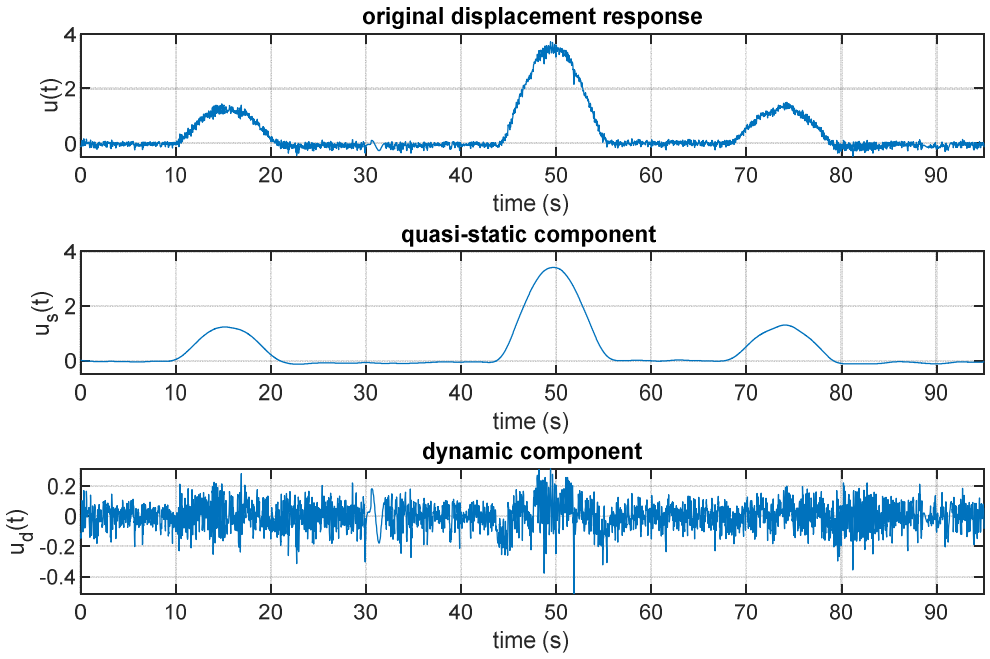

Figure 2. Decomposition of bridge displacement responses under moving load.

As mentioned in Section 2, the proposed DTIR indicator is extracted from the quasi-static component. In this study, a lowpass filter is adopted to separate the low-frequency quasi-static displacement from the high-frequency dynamic component and measurement noise. The selection of an appropriate lowpass filter cut-off frequency depends on the characteristics of the original signal, and in this case, it is set to half of the bridge's fundamental frequency. It is important to note that there are other methods commonly used for signal decomposition, such as singular spectrum analysis, empirical mode decomposition, and variational mode decomposition.

3.3. Peak value detection

As shown in Equation (5), the vehicle-induced bridge displacement amplitude is the key to estimating the proposed DTIR indicator. The displacement responses of each girder simultaneously increase and reach their peak values when the vehicle crosses over the displacement measurement location. The transverse displacement influence ratio between any two girders can be estimated by calculating the peak value ratio of the selected girder pair. For a single vehicle trip measurement, it is easy to manually determine the peak in the displacement responses under traffic load. However, in long-term health monitoring, it is necessary to automatically extract all the peaks of each girder from the displacement measurement over a period of time.

The threshold such as the minimum peak value and the minimum peak distance can be used to assist extractions. The minimum peak value is used to remove the local peaks that were induced by ignorable small car or measurement noise. The minimum peak distance can be specified to ignore smaller peaks that may occur in close proximity to a large local peak. Figure 3 illustrates the mid-span deflection of four girders bridge corresponding to two round trips. As shown in Figure 5, the bridge has two traffic lanes. In each round trip, vehicle departs from the left approach span via Lane two and returns via Lane one. When the vehicle presents on Lane two, the vehicle load is mainly undertaken by girder 3 and girder 4, and thus the deflection of these two girders is higher than that of girder 1 and girder 2. As illustrated in Figure 3, all the real vehicle-induced displacement peaks are higher than 1mm, and the horizontal distance between any two adjacent peaks is longer than 15 s. Therefore, the minimum peak value and the minimum peak distance can be set to 1mm and 15 s, respectively. It is noted that the peak values detection can be conveniently conducted using the Python and MATLAB signal processing toolbox. In Figure 3, for example, $peak_{g1}^{i}$ represents the *i*-th peak identified from the displacement response of girder 1 subjected to a trip of moving load.

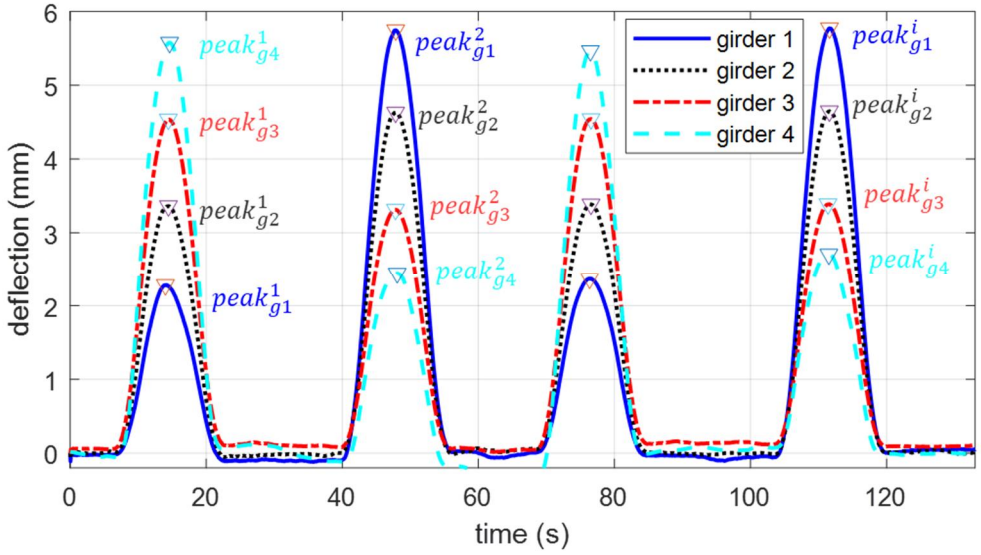

Figure 3. Peak value detection of bridge displacement responses under moving load.

3.4. Damage detection based on DTIR indicator

The displacement peak values of a multi-girder beam bridge subjected to operational conditions forms up the following dataset **D**:

$$\boldsymbol{D} = \begin{bmatrix} \boldsymbol{peak}_{g1} \\ \boldsymbol{peak}_{g2} \\ \vdots \\ \boldsymbol{peak}_{g4} \end{bmatrix} = \begin{bmatrix} peak^1_{g1} & peak^2_{g1} & \cdots & peak^n_{g1} \\ peak^1_{g2} & peak^2_{g2} & \cdots & peak^n_{g2} \\ \vdots & \vdots & \ddots & \vdots \\ peak^1_{g4} & peak^2_{g4} & \cdots & peak^n_{g4} \end{bmatrix} \tag{7}$$

For a four-girder beam bridge that has undergone n trips of moving vehicle load tests, the dimension of matrix **D** is 4 × n. Each column of matrix **D** can be used to estimate the DTIR as defined in Section 2. Consequently, the DTIR indicator between every two adjacent girders can be expressed as follows:

$$\boldsymbol{DTIR} = \begin{bmatrix} \boldsymbol{DTIR}_{g1,g2} \\ \boldsymbol{DTIR}_{g2,g3} \\ \boldsymbol{DTIR}_{g3,g4} \end{bmatrix} = \begin{bmatrix} DTIR^1_{g1,g2} & DTIR^2_{g1,g2} & \cdots & DTIR^n_{g1,g2} \\ DTIR^1_{g2,g3} & DTIR^2_{g2,g3} & \cdots & DTIR^n_{g2,g3} \\ DTIR^1_{g3,g4} & DTIR^2_{g3,g4} & \cdots & DTIR^n_{g3,g4} \end{bmatrix} \tag{8}$$

The dimension of ***DTIR*** matrix is 3 × n, in which, the element is estimated from the peak value ratio of adjacent girder pair. For example, $DTIR^i_{g1,g2} = \frac{peak^i_{g1}}{peak^i_{g2}}$. It should be noted that the peak value ratio $DTIR^i_{g1,g3}$, $DTIR^i_{g1,g4}$ and $DTIR^i_{g2,g4}$ can also be obtained; however, they are not included in this study. This is because the load distribution pattern between two adjacent girders will change significantly when the connection stiffness between the adjacent girders is altered. Therefore, the damage indicator $DTIR^i_{g1,g2}$, $DTIR^i_{g2,g3}$ and $DTIR^i_{g3,g4}$ will be more sensitive to structural damage (transverse connection stiffness reduction) than $DTIR^i_{g1,g3}$, $DTIR^i_{g1,g4}$ and $DTIR^i_{g2,g4}$.

The overall framework of the proposed bridge damage detection using measured bridge displacement is illustrated in Figure 4. The system utilizes a video camera to measure the

vertical displacement responses of the bridge under vehicle load. The camera can be set up at a distance from the bridge for short-term measurements or fixed on the bridge pier for long-term measurements. For short-span bridges, the video of a specific bridge cross-section can be selected as the Region of Interest (ROI) to measure the vertical displacement at different transverse locations on the deck. For long-span bridges, multiple synchronized cameras with zoom lenses can be used, with each camera targeting one transverse location to enhance image resolution.

The main contributions and novelties of this study lie in the following aspects: i) a reliable damage sensitive feature is directly extracted from the measured bridge displacement in a fully data-driven manner and does not require any information regarding the traffic conditions; ii) theoretical derivations have proven that the proposed damage feature is sensitive to structural local damage while being robust to variations in vehicle weight and speed.

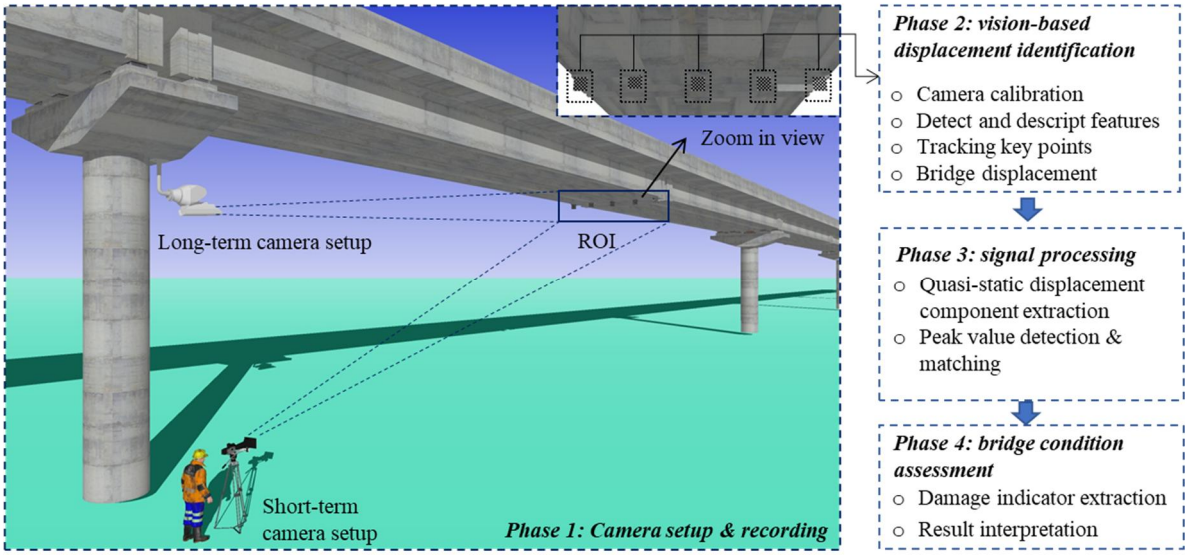

Figure 4. Framework of the computer vision-based bridge health monitoring system.

4. Experiment study

4.1. Experimental setup and instrumentation

A series of drive-by experiments was performed on a multi-girder beam bridge, as depicted in Figure 5. The bridge is supported by steel bars at both ends and has a span length of 4 meters. To account for the approaching stage, a length of 0.6 meters is considered on both the left and right sides of the main span. To increase the deadweight of the bridge and consequently lower the fundamental frequency to approximately 5 Hz, three 5 kg mass blocks were attached at specific locations along the span. The chosen locations were at L/4 (one-fourth of the span length), L/2 (half of the span length), and 3L/4 (three-fourths of the span length), respectively.

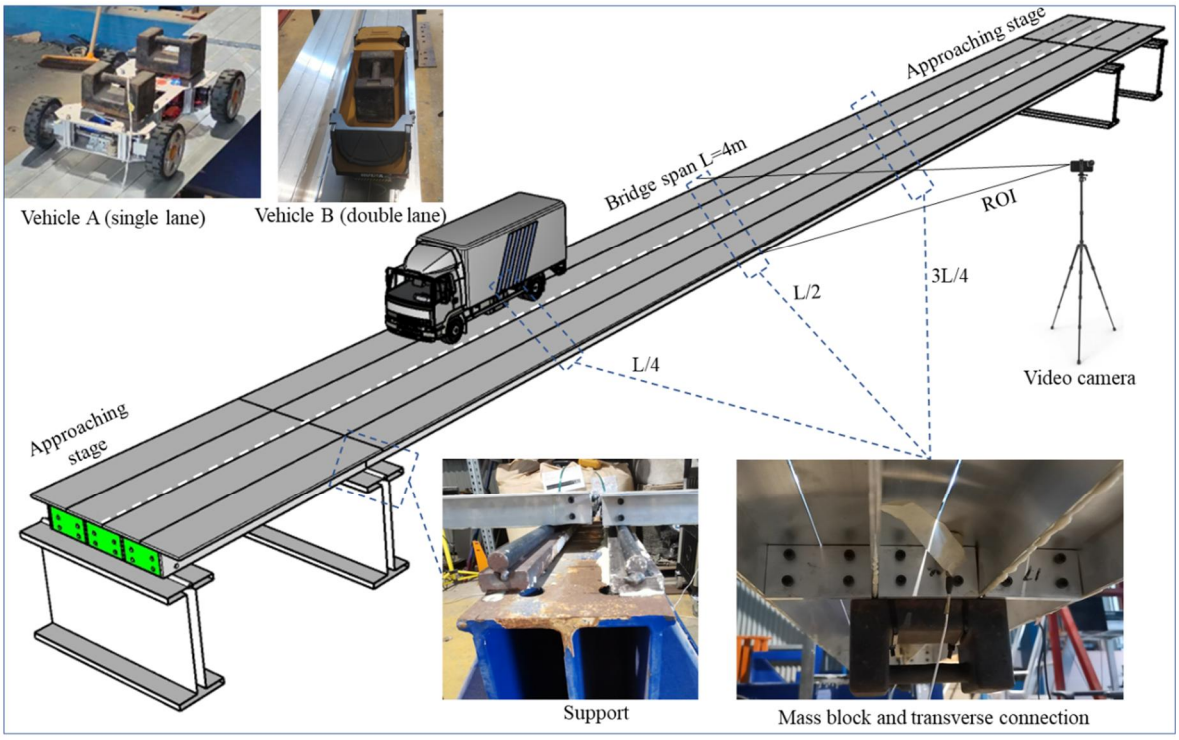

Figure 5. Schematic of the instrument layout.

Figure 6 presents the layout of sensors, the bottom view, and the cross section of the representative section of the bridge model. In particular, the bridge consists of four aluminium Tee-section girder G1~G4 with a width and height of 100 mm and 50 mm, respectively. The width of multi-girder beam bridge is 400 mm. As shown in Figure 6, transverse connection C1~C9 were considered at L/4, L/2 and 3L/4 span to establish the transverse connection between girders. Two laser displacement sensors were installed to measure the vertical displacement at the L/2 and 3L/4 spans. Six single-axis accelerometers were placed on the bottom of the bridge along the longitudinal direction. As shown in the top-left of Figure 5, two vehicle models with widths of 358 mm (vehicle A) and 150 mm (vehicle B) were utilized to simulate single and double traffic lane scenarios. In practical applications, the vehicle speed and vehicle weight may vary, and they could affect the performance of damage detection methods. Therefore, variations in vehicle speed and weight are considered to evaluate the robustness of the proposed damage feature. For vehicle A, three vehicle weights were considered, including unloaded (6.12 kg), add 5 kg (11.12 kg), and add 10 kg (16.12 kg). For each vehicle weight, three levels of vehicle speeds were considered via the remote control. The vehicle speeds corresponding to slow, medium, and fast modes are approximately 0.217 m/s, 0.355 m/s, and 0.505 m/s, respectively. According to the non-dimensional speed parameter $\gamma = \frac{v}{2 \times f_{b1} L}$, these three vehicle speeds are respectively equivalent to a full-scale vehicle speed of 14 km/h, 23 km/h, and 33 km/h for a bridge with a span of 100 m and a fundamental frequency of f_{b1}= 4 Hz. In this equation, v and L represent the vehicle speed and bridge span, respectively. The weight of vehicle B in the unloaded state is 2.63 kg. Two vehicle weights, including an additional 5 kg (7.63 kg) and an additional 10 kg (12.63 kg), were considered. The speed of vehicle B is approximately

0.38 m/s. The number of round trips corresponding to different combinations of structural condition, vehicle model, vehicle weight, and speed is listed in Table 1. Overall, 976 trips of drive-by data were recorded. A smartphone camera with tripod is placed underneath the bridge and target to the midspan of the bridge girder. In the experimental setup, the camera is approximately perpendicular to the target plane. The video is recorded with a resolution of 1920 × 1080 and a sampling rate of 60 fps, without distortion. In this test, the bridge motion under the moving load is predominantly vertical displacement. The changes in view and distance between the camera and the target are negligible during the vibration. Therefore, the homography transformation mentioned in Section 3.1 is suitable for obtaining the scale factor.

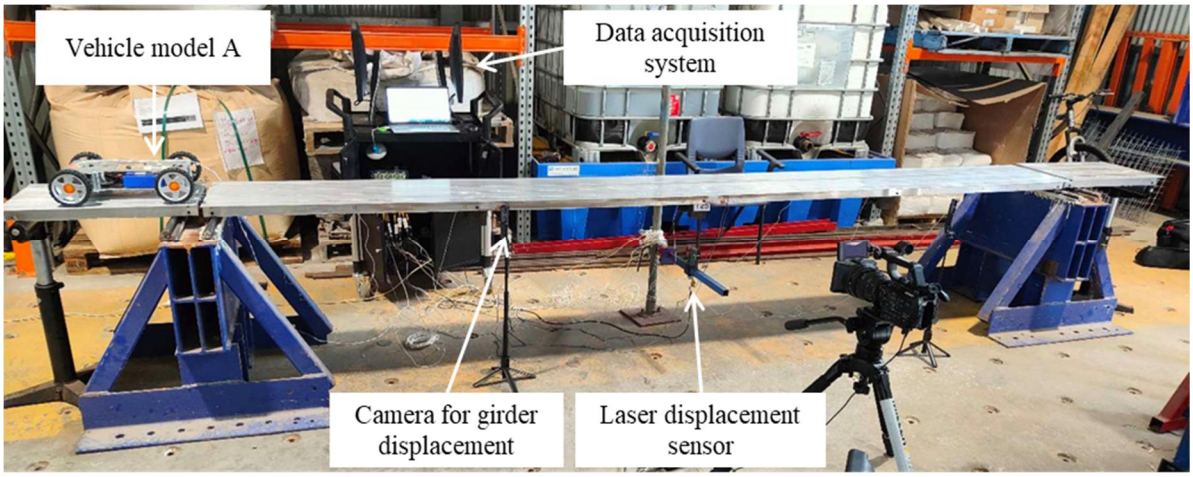

Figure 6. Overview of test structure.

4.2. Damage scenarios

Three structural conditions were considered, including the healthy state (damage scenario 0), the removal of transverse connection C6 as shown in Figure 7 (damage scenario 1), and the removal of transverse connections C3&C6 (damage scenario 2). Considering damage occurring at the transverse connections of a multi-girder beam bridge is common and of practical significance. For example, it was reported that there was a substantial loss of transverse bending stiffness in the adjacent box-beam connection of a precast prestressed concrete box-beam bridge after nearly 25 years of service life [27]. It was also reported that the transverse connection stiffness of a multiple-girder bridge had degraded greatly after operating for 19 years [28]. Reference [29] also highlighted that field investigation shows that severe damage to the transverse connectivity component occurred during its service life, which will result in deterioration of the bridge's mechanical performance. In this study, modal analysis was conducted using the bridge acceleration responses when the vehicle left the bridge. The bridge's fundamental frequencies corresponding to the three different structural conditions were found to be 5.56593 Hz, 5.51775 Hz, and 5.51545 Hz, respectively. The relative changes in the fundamental frequencies corresponding to damage scenario 1 and scenario 2 were 0.865% and 0.907%, respectively. This result suggests that the removal of transverse connections only causes minor local damage, resulting in a relatively small reduction in the overall stiffness of the bridge.

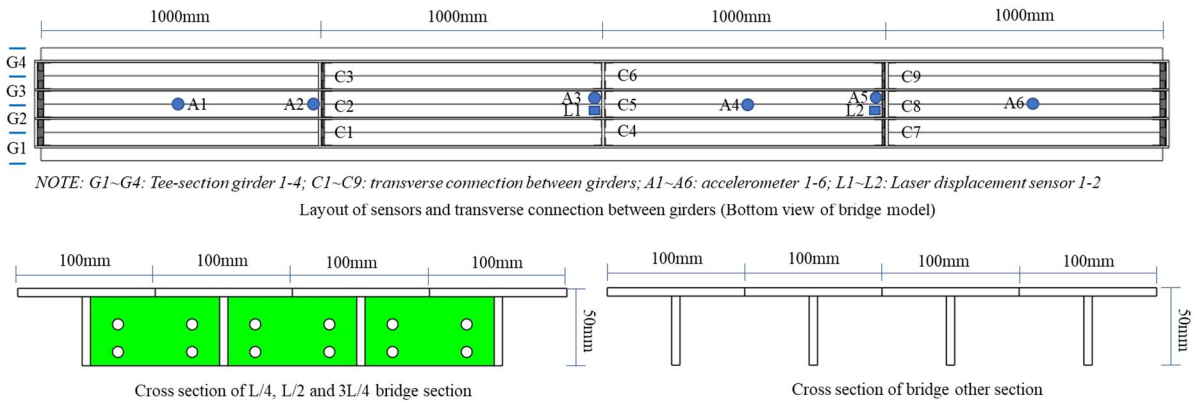

Figure 7. Plan view and cross sections of the bridge model.

Table 1. List of drive-by test scenarios.

	Description		Damage scenario 0	Damage scenario 1	Damage scenario 2
Vehicle model	Vehicle mass	Vehicle speed	Health	Remove C6	Remove C3&C6
Vehicle A: single lane	Unloaded	slow	10 trips	8 trips	30 trips
		medium	40 trips	40 trips	42 trips
		fast	36 trips	20 trips	40 trips
	Add 5 kg	slow	12 trips	10 trips	36 trips
		medium	46 trips	40 trips	42 trips
		fast	40 trips	40 trips	42 trips
	Add 10 kg	slow	14 trips	10 trips	30 trips
		medium	40 trips	40 trips	34 trips
		fast	40 trips	40 trips	40 trips
Vehicle B: double lane	Add 5 kg	-	20 trips	18 trips	20 trips
	Add 10 kg	-	18 trips	18 trips	20 trips

4.3. Estimation of DTIR

This section follows the procedures outlined in Section 3 for estimating the transverse influence ratio of displacement from the experimental structure. The first step involves identifying the displacement responses of the four girders using the SIFT-FLANN-based method. Figure 8 illustrates the results of this process. It can be observed from Figure 8(a) that feature points on the vertical web of the girders were detected. Figure 8(b) demonstrates that the feature points were successfully matched with minimal mismatches occurring outside the vertical web regions of the girders.

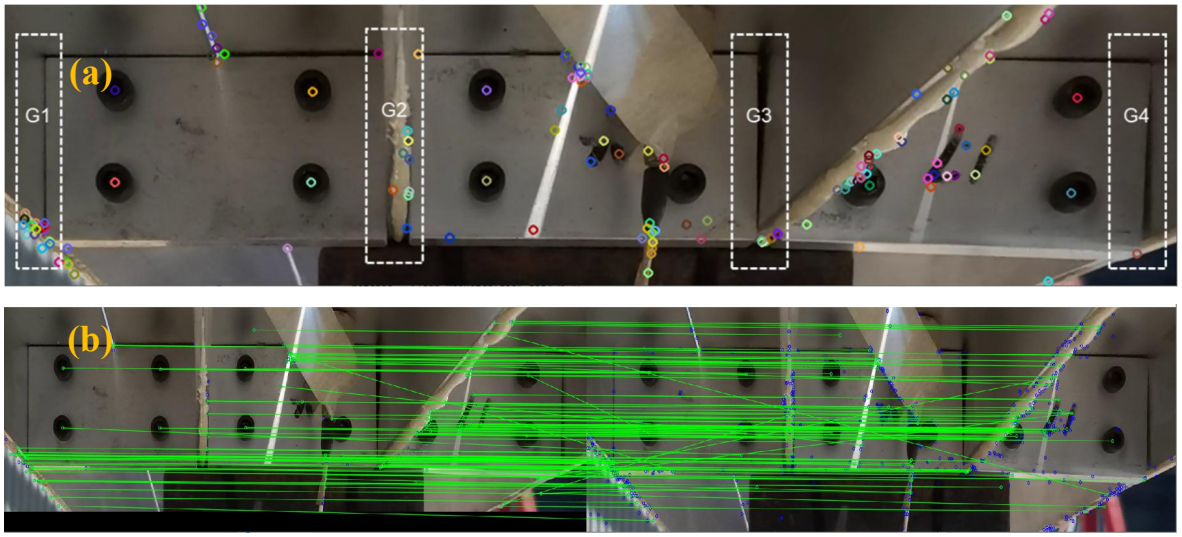

Figure 8. (a) Feature points detected from SIFT and **(b)** feature points matched from FLANN algorithm.

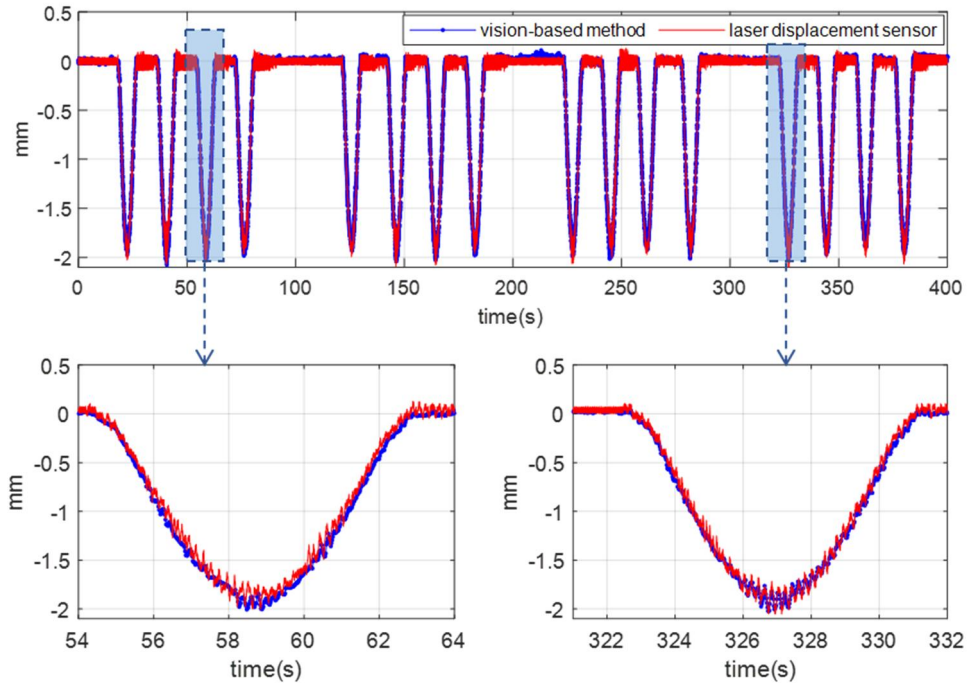

Figure 9. Comparison of displacement measurement from computer vision-based method and laser displacement sensor.

To assess the accuracy of the computer vision-based displacement identification method, a video captured from Vehicle A (unloaded and fast speed mode) while passing over the healthy bridge serves as an example for the evaluation. Figure 9 presents a comparison between the displacements identified from a laser displacement sensor and those identified using the SIFT-FLANN-based method. The bottom panel of Figure 9 consists of two subfigures showing a zoomed-in view of the displacement at two small time windows. The correlation coefficient between the two time histories is 0.9969, indicating a strong relationship. Additionally, the Root-mean-square error between the two sets of data is 0.0586,

signifying a small deviation. The displacement responses obtained from the video align well with the measurements obtained by the laser displacement sensor. This outcome validates the accuracy of the vision-based displacement measurement method and confirms the correctness of the scale factor determination method employed.

It is noted that the maximum displacement presented in Figure 9 is about 2 mm, which corresponds to 1/2000 of the bridge's main span. This deflection-span ratio is in line with that of a real bridge subjected to operational traffic load.

The time domain displacement presented in Figure 9 is transformed into the frequency domain (as shown in Figure 10) using fast Fourier transform. Overall, the amplitude of the frequency spectrum shows a decreasing trend. It can be observed in Figure 10 that the amplitude of the quasi-static component is two orders of magnitude higher than that of the bridge's fundamental frequency. In particular, the amplitude of the quasi-static component at 0 Hz is 0.657699, whereas at the bridge's fundamental frequency of 5.5 Hz the amplitude is 0.00548. This indicates that the bridge displacement response under a moving load is dominated by the quasi-static component. This observation confirms that the damage indicator DTIR derived from the bridge's quasi-static displacement is more reliable than those defined from the modal parameters from the displacement response.

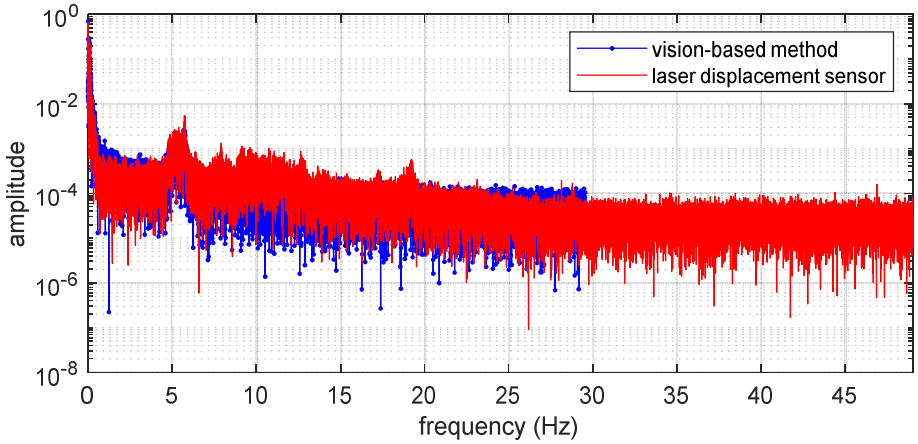

Figure 10. Frequency spectrum of bridge mid-span displacement under the moving load.

Now that the bridge displacement of four girders corresponding to the drive-by test scenarios have been measured from the computer vision-based method, the damage feature *DTIR* defined in Equation (8) can be estimated by following the procedure detailed in Section 3.

In order to assess the suitability of computer vision-based displacement identification methods for long-term SHM applications, it is essential to evaluate their video processing efficiency. In this study, a 10-minute video with a frame rate of 60 fps was employed to test the processing efficiency of the SIFT-FLANN-based method. The average processing frames per second (fps) for different sizes of square ROIs were analyzed and presented in Figure 11. The ROIs considered in the evaluation were 100 pixels × 100 pixels, 200 pixels × 200 pixels, 300 pixels × 300 pixels, and 400 pixels × 400 pixels, respectively. The result shows that the video can be processed at 60 fps (near real time) with ROI of 100 pixels × 100 pixels and above 30 fps with ROI of 200 pixels × 200 pixels. It is noted that a frame rate of 30 fps and

a ROI of 200 pixels × 200 pixels is sufficient to capture the quasi-static displacement component of civil engineering structure subjected to normal operational condition. Therefore, the displacement tracking method employed in this study is suitable for long term bridge SHM. It is noted that the computations are performed on a desktop with an AMD Ryzen 7 5800U with Radeon Graphics and 16 GB RAM.

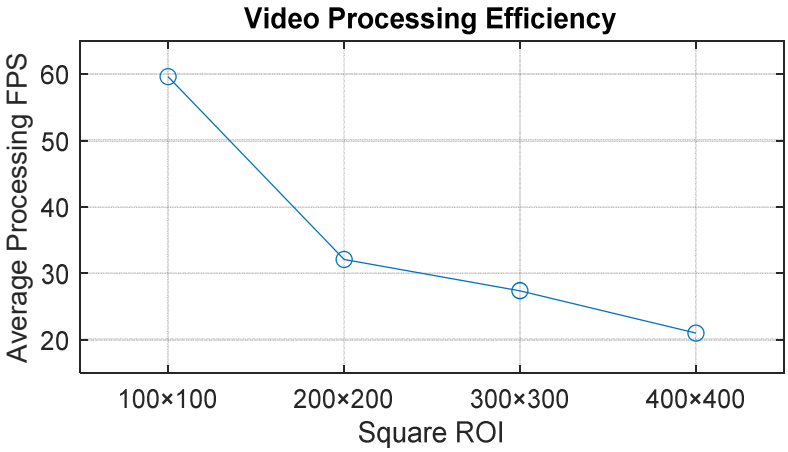

Figure 11. The average processing frames per second (fps) for different sizes of square ROIs.

4.4. Damage detection results

As shown in Figure 12, two vehicle models, namely vehicle A and vehicle B, were used to simulate the bridge with single and double traffic lane configurations. In particular, the moving vehicle tests conducted by vehicle A and vehicle B consisted of 862 trips and 114 trips, respectively. The damage detection results for vehicle A and vehicle B are presented in Section 4.4.1 and Section 4.4.2, respectively. In the case of the double traffic lane configuration, vehicle model B will depart from the left approach span via Lane two and return via Lane one.

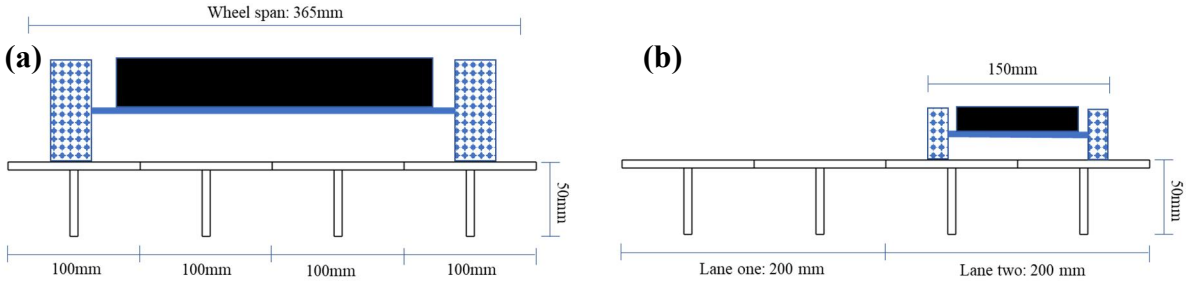

Figure 12. Side view of **(a)** single and **(b)** double traffic lane configuration.

4.4.1 Single traffic lane configuration

As illustrated in Figure 12(a), the vehicle wheel load is directly applied to girder 1 and girder 4, and then transferred to girder 2 and girder 3 via the transverse connection block between the girders. The DTIR indicator between any two adjacent girder pairs, along with their 95% confidence intervals, is presented in Figure 13. In the healthy state, the mean values of the

DTIR indicator corresponding to girder pair 1-2, girder pair 2-3, and girder pair 3-4 are 0.9939, 1.0325, and 0.9376, respectively. According to the definition, a DTIR indicator close to 1 means that the vehicle load is evenly distributed among the four girders. A shift in the DTIR indicator was observed in all three adjacent girder pairs with the introduction of structural damage. For damage scenario 1, the mean values of the DTIR indicator corresponding to girder pair 1-2, girder pair 2-3, and girder pair 3-4 changed by 3.52%, 2.31%, and 6.30%, respectively. For damage scenario 2, the mean values of the DTIR indicator corresponding to girder pair 1-2, girder pair 2-3, and girder pair 3-4 changed by 10.05%, 5.45%, and 21.50%, respectively. In both damage scenarios, the maximum change in the DTIR indicator was observed in girder pair 3-4. In the test implementation, the removal of transverse connection C6 (damage scenario 1) and C3&C6 (damage scenario 2) introduces two levels of transverse stiffness reduction between girder 3 and girder 4, which agrees well with the identification results. The damage occurring between girder pair 3-4 affects the load force transmission path and thus introduces loading redistribution among the other girder pairs.

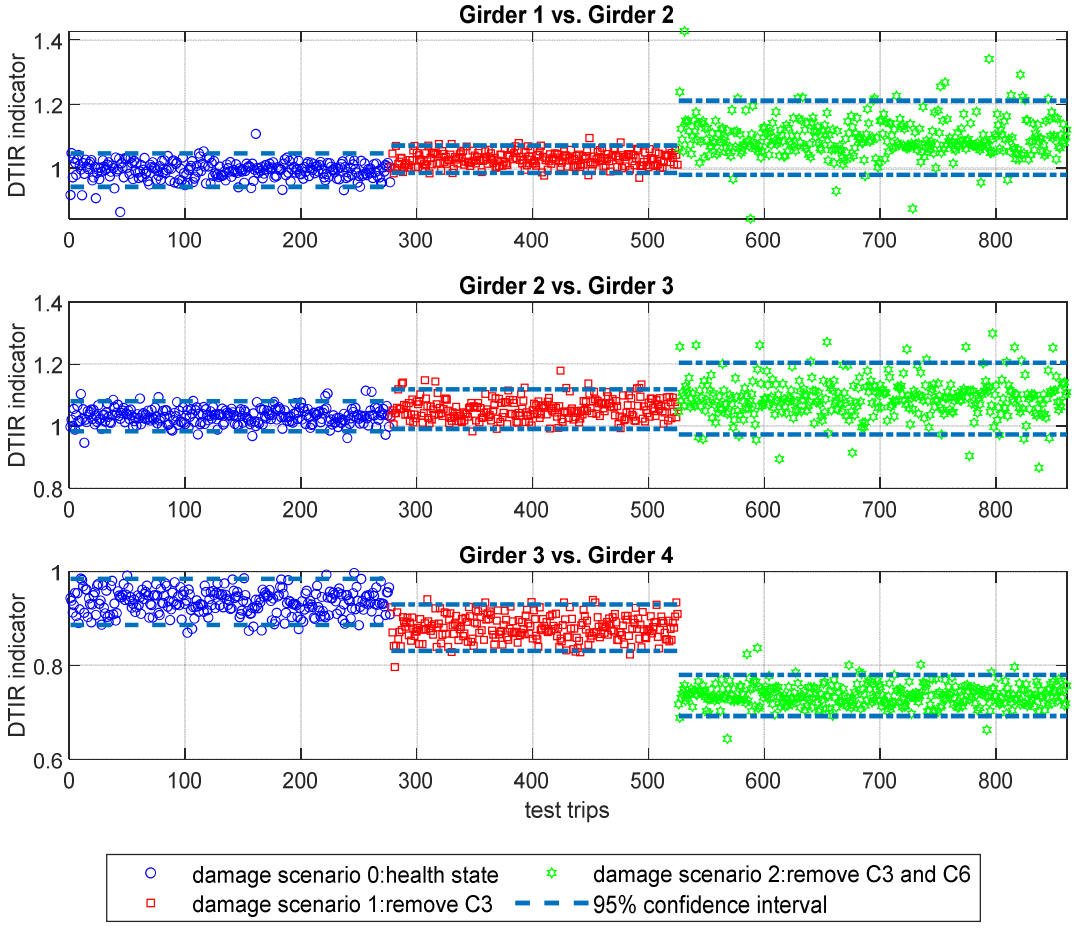

Figure 13. Damage identification result of single traffic lane configuration.

In field applications, vehicle information such as vehicle speed and weight is often unknown and subject to variation. Therefore, it is necessary to evaluate the robustness of the proposed method to these factors. To this end, the identification results of damage scenario

2 corresponding to 9 different combinations of vehicle speed and vehicle weight were sorted out and presented in Figure 14. It is observed that the variation of vehicle weight and speed has limited effects on the proposed DTIR indicator, and the three structural conditions can be well distinguished for each combination of vehicle state.

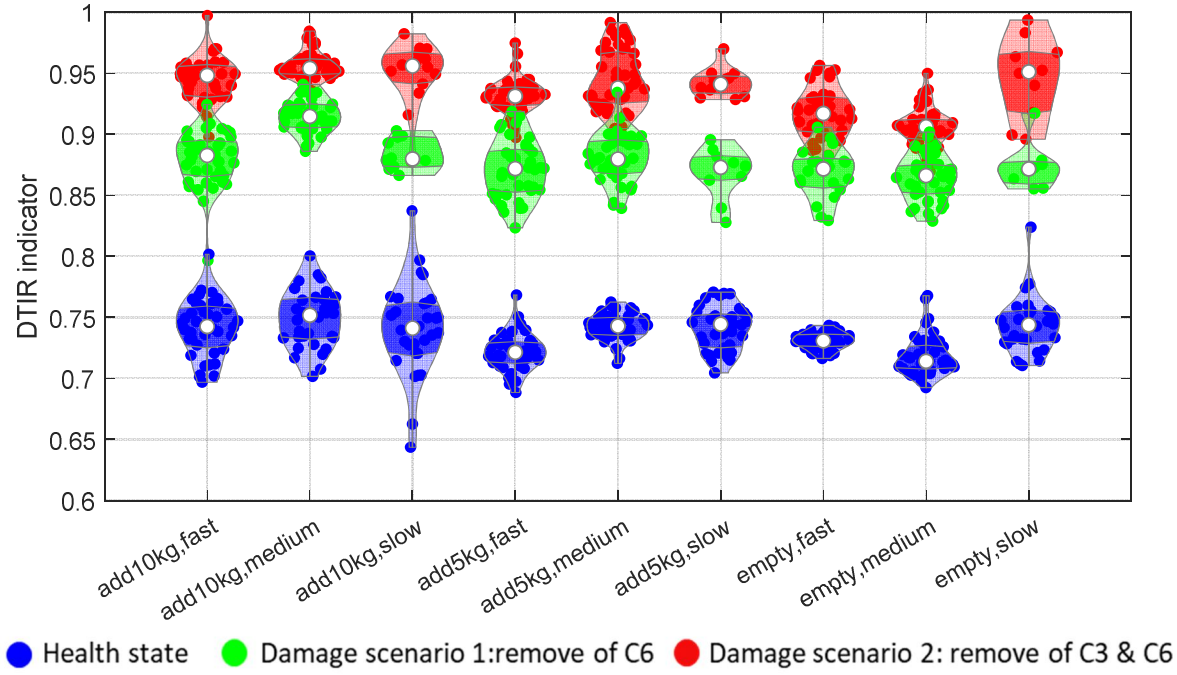

Figure 14. Violin plot of DTIR indicator corresponding to different vehicle load and vehicle speed.

4.4.2 Double traffic lane configuration

As illustrated in Figure 12(b), the wheel load of vehicle B is directly applied to either girders 1 and 2 or girders 3 and 4, and then transferred to the other two girders via the transverse connection block between the girders. In contrast to the results of the single traffic lane configuration presented in Figure 13, the damage identification result of the double traffic lane configuration, shown in Figure 15, forms two clusters. This fact can be explained by the theoretical derivation of the DTIR indicator defined in Equation (5). It can be observed from Equation (5) that the transverse displacement influence ratio is related to the structural condition and the vehicle's transverse location, while it is independent of the weight and the longitudinal location of the vehicle. For the double traffic lane configuration, there will be two vehicle transverse locations (the central line of each traffic lane) by concentrating the vehicle wheel load to the center of gravity. Consequently, for a bridge bearing m traffic lanes, the DTIR indicator forms m clusters.

As a vehicle crosses over the bridge, the girders directly under the wheels receive the most load, while the other girders farther away from the loaded lane receive less load. Taking the top subfigure of Figure 15 as an example, the cluster of DTIR indicators greater than 1 is formed from the data when the vehicle is moving on traffic lane one, while the cluster of DTIR indicators smaller than 1 is formed from the data when the vehicle is moving on traffic

lane two. It is evident that the upper cluster of DTIR indicators between girder 3 and girder 4 significantly shifted upward with the introduction of structural damage. In particular, the mean value of the upper cluster of DTIR indicators corresponding to girder pair 3-4 changed by 30.23% (damage scenario 1) and 89.60% (damage scenario 2). The damage identification results also indicate that the structural damage is most likely to have occurred between girders 3 and 4.

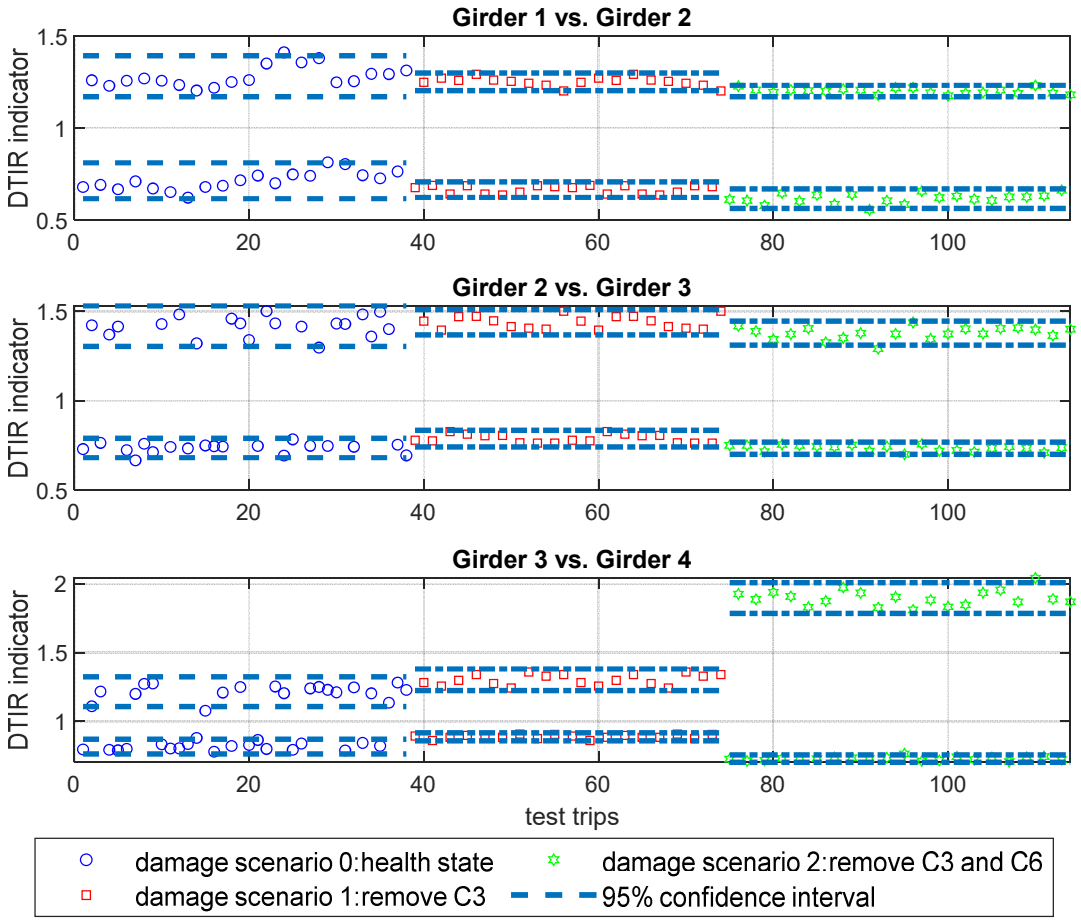

Figure 15. Damage identification result of double traffic lane configuration.

4.5. Discussion

The results provided evidence that the proposed damage feature, extracted from the computer vision-based bridge displacement responses, consistently achieved successful detection and localization of damage, even in the presence of varying vehicle weights and speeds. Compared to existing displacement influence line-based damage detection methods, the proposed method is fully data-driven and does not rely on traffic information. The study results demonstrated that the damage feature, extracted from the computer vision-based bridge displacement responses, consistently yielded successful outcomes in both detecting and localizing structural damage. The proposed damage feature is sensitive to local structural damage while remaining robust against variations in vehicle weight and speed. In comparison to existing displacement influence line-based damage detection methods, the proposed method is fully data-driven and does not require any information regarding traffic conditions.

The proposed damage feature, DTIR, can be integrated with other more advanced displacement measurement methods to evaluate the bridge condition under operational conditions. Consequently, this study presents a cost-effective, easily deployable, and scalable approach for structural health monitoring of bridges. However, it is important to note that the findings presented in this paper are based on laboratory test results conducted on a scaled bridge. As a result, there are still certain gaps that need to be addressed in order to extend the proposed approach to practical applications. To further enhance the applicability of the method, the following discussions and suggestions are provided for filling these gaps:

(1) In the experimental test, only one vehicle is on the bridge. According to Reference [30], about 300 out of 5000 vehicles per day on the cable-stayed bridge meet this requirement. Therefore, the proposed method is applicable from a long-term SHM perspective. However, in practical situations, the traffic pattern is much more complex. Hence, suitable signal pre-processing techniques should be adopted to sort out the data when only one vehicle is present on the bridge [30]. Alternatively, a traffic monitoring camera can be installed to identify the traffic flow. Despite the need for an additional camera to collect traffic information, the proposed method still outperforms the displacement influence line-based damage detection method. This is because reconstructing the bridge displacement influence line requires knowledge of the vehicle axle load. Consequently, additional weight-in-motion technology should be deployed to gather this information.

(2) The structural damage considered in this study is the reduction of transverse connection stiffness, which is a common type of damage in multi-girder beam bridges. The applicability of the proposed method to other types of structural damage, such as girder bending stiffness reduction as well as different bridge types, should be further studied.

(3) In this study, videos corresponding to nearly a thousand trips of moving vehicle tests were recorded and analyzed, which is sufficient to demonstrate the accuracy and efficiency of the introduced computer vision-based displacement identification method, as well as the feasibility of the proposed damage detection method. However, the videos are stored locally and processed offline. In long-term structural health monitoring applications, it is more practical to develop a vision sensor node to process the video stream in real-time.

(4) In the experimental study, the bridge is tested with both single and double traffic lane configurations. To generalize the proposed method to bridges with more than two traffic lanes, a Gaussian mixture model (GMM) can be adopted to cluster the defined DTIR indicator. The number of clusters would be equal to the number of traffic lanes. Then, the fitted parameters of the GMM, such as the mean value and standard deviation of each cluster, can be employed as the damage index. To confirm this, GMM models with cluster numbers 1 and 2 were adopted to fit the DTIR indicator estimated from single and double traffic lanes, respectively. The fitting results are presented in Figures 16–17. It is observed that the DTIR indicator corresponding to single traffic lane and double traffic lanes can be well-fitted by the GMM models with cluster numbers 1 and 2. The DTIR indicator estimated from Girder pair 3-4 shows the most obvious shift.

(5) In practical field applications, cameras are often far away from the structure, requiring long focal lengths to capture high-resolution images. However, this reduces the field of

view, potentially prevents simultaneously capturing the adjacent beams. One possible solution to measure multi-point displacement responses is to develop a full-field displacement measurement method by roving the camera along the bridge at different locations. The images from multiple cameras or a single camera at different locations can be used to obtain the full -field displacement measurement for modal identification and condition monitoring of the whole structure [15].

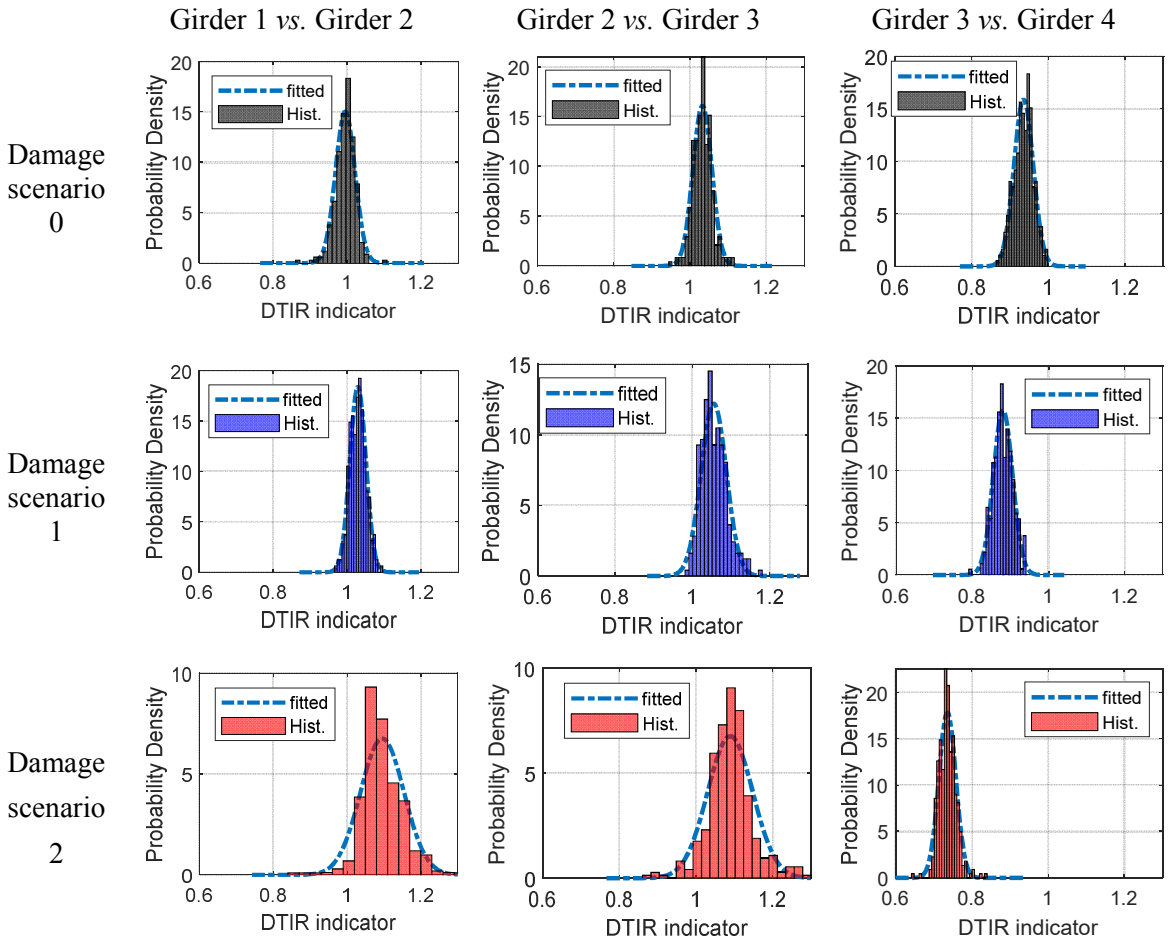

Figure 16. Fitted GMM model of single traffic lane configuration.

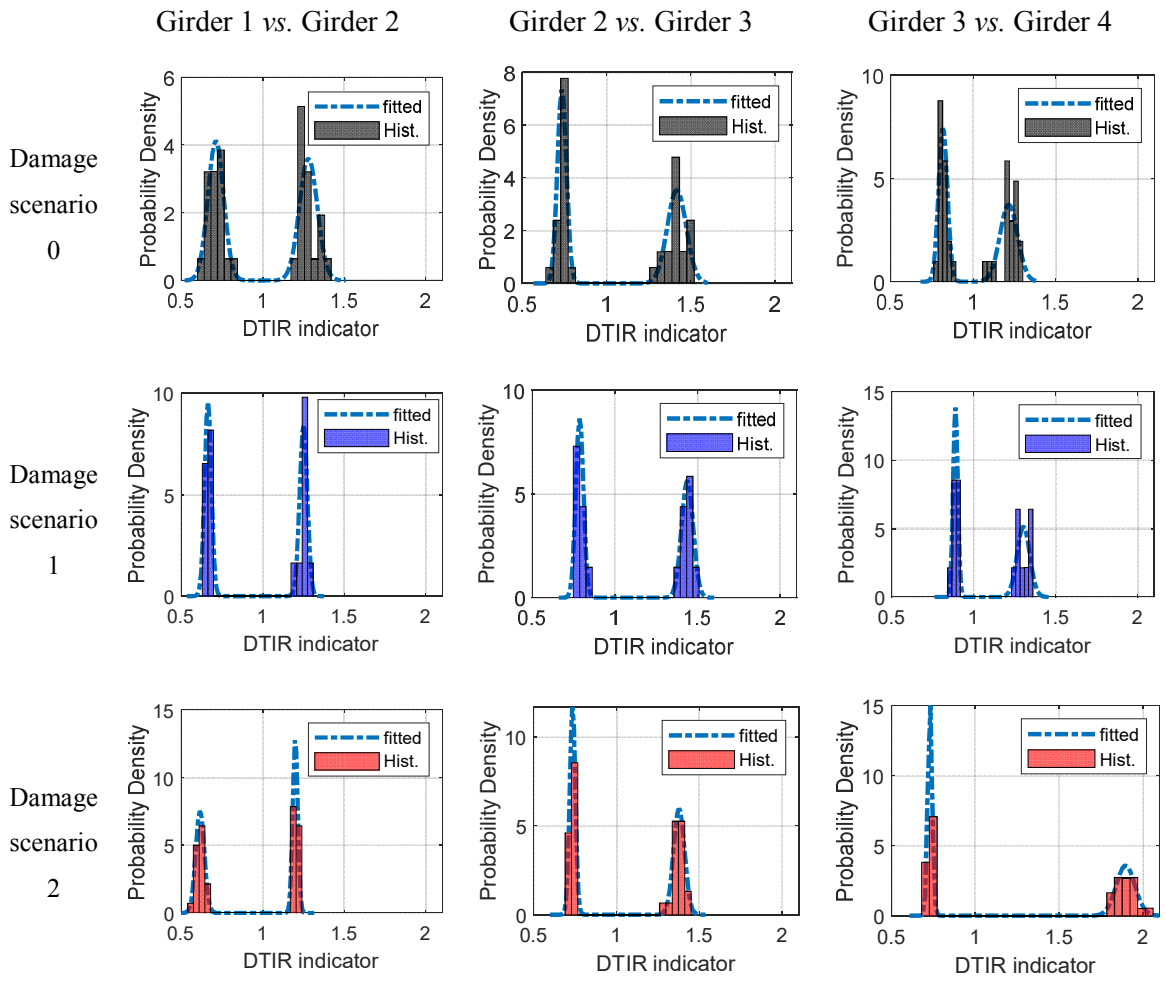

Figure 17. Fitted GMM model of double traffic lanes configuration.

5. Conclusions

This paper presents a novel approach for bridge damage detection, which relies on the ratio of vehicle-induced displacement obtained from two adjacent girders. The proposed method employs computer vision-based displacement measurement techniques to accurately measure the displacements. The main conclusions are remarked as follows:

(1) The damage indicator, DTIR, is theoretically defined following the bridge influence line/surface theory. Theoretical derivation proves that DTIR indicator is only related to the structural condition and the transverse position of a vehicle over the deck, while independent of the variation of vehicle weight and speed.

(2) The DTIR-based bridge damage detection framework is systematically proposed. The DTIR indicator can be precisely estimated from computer vision-based displacement measurement and related practical signal processing methods, including quasi-static displacement component extraction, peak value detection. The accuracy and efficiency of the employed computer vision-based displacement tracking algorithm is carefully evaluated.

(3) Comprehensive experimental studies verified that the developed DTIR indicator can successfully identify the reduction of structural transverse stiffness between girders under

different vehicle speed and weight. In particular, the introduced two structural damage scenarios just caused 0.865% and 0.907% change to bridge fundamental frequency. The DTIR damage indicator corresponding to these two damage scenarios changed more than 6% and 21%, respectively. This result suggests that the minor local damage that introduced relatively small reduction in the overall stiffness of the bridge is possible to be identified by using the proposed method.

The limitation of extending the proposed method to practical applications is identified. Furthermore, future study directions are suggested to maximize the potential of the proposed method to long-term SHM application.

Acknowledgments

This study was funded by the Australian Research Council Future Fellowship FT190100801, "Innovative Data Driven Techniques for Structural Condition Monitoring".

Conflicts of interests

The authors declared no potential conflicts of interest with respect to the research, authorship, and publication of this article.

Authors' contribution

Zhen Peng: Conceptualization, Methodology, Validation, Formal analysis, Investigation, Data curation, Writing – original draft, Visualization. **Jun Li:** Conceptualization, Methodology, Investigation, Writing – review & editing, Supervision, Funding acquisition. **Hong Hao:** Conceptualization, Methodology, Investigation, Writing – review & editing, Supervision.

References

[1] Hao H, Bi K, Chen W, Pham TM, Li J. Towards next generation design of sustainable, durable, multi-hazard resistant, resilient, and smart civil engineering structures. *Eng. Struct.* 2023, 277:115477.

[2] Peng Z, Li J, Hao H. Structural damage detection via phase space based manifold learning under changing environmental and operational conditions. *Eng. Struct.* 2022, 263:114420.

[3] Peng Z, Li J, Hao H, Xin Y. High - resolution time - frequency representation for instantaneous frequency identification by adaptive Duffing oscillator. *Struct. Control Health Monit.* 2020, 27:e2635.

[4] Peng Z, Li J, Hao H, Yang N. Mobile crowdsensing framework for drive-by-based dense spatial-resolution bridge mode shape identification. *Eng. Struct.* 2023, 292:116515.

[5] Peng Z, Li J, Hao H. Data driven structural damage assessment using phase space embedding and Koopman operator under stochastic excitations. *Eng. Struct.* 2022, 255:113906.

[6] Peng Z, Li J, Hao H. Development and experimental verification of an IoT sensing system for drive-by bridge health monitoring. *Eng. Struct.* 2023, 293:116705.
[7] Deng J, Singh A, Zhou Y, Lu Y, Lee VC-S. Review on computer vision-based crack detection and quantification methodologies for civil structures. *Constr. Build. Mater.* 2022, 356:129238.
[8] Dong C-Z, Catbas FN. A review of computer vision–based structural health monitoring at local and global levels. *Struct. Health Monit.* 2021, 20:692-743.
[9] Khuc T, Catbas FN. Structural identification using computer vision–based bridge health monitoring. *J. Struct. Eng.* 2018, 04017202.
[10] Dong C-Z, Bas S, Catbas FN. Investigation of vibration serviceability of a footbridge using computer vision-based methods. *Eng. Struct.* 2020, 224:111224.
[11] Martini A, Tronci EM, Feng MQ, Leung RY. A computer vision-based method for bridge model updating using displacement influence lines. *Eng. Struct.* 2022, 259:114129.
[12] Feng D, Feng MQ. Computer vision for SHM of civil infrastructure: From dynamic response measurement to damage detection–A review. *Eng. Struct.* 2018, 156:105-117.
[13] Spencer Jr BF, Hoskere V, Narazaki Y. Advances in computer vision-based civil infrastructure inspection and monitoring. *Eng.* 2019, 5:199-222.
[14] Bhowmick S, Nagarajaiah S. Identification of full-field dynamic modes using continuous displacement response estimated from vibrating edge video. *J. Sound Vib.* 2020, 489:115657.
[15] Tan D, Li J, Hao H, Nie Z. Target-free vision-based approach for modal identification of a simply-supported bridge. *Eng. Struct.* 2023, 279:115586.
[16] Wang M, Ao WK, Bownjohn J, Xu F. Completely non-contact modal testing of full-scale bridge in challenging conditions using vision sensing systems. *Eng. Struct.* 2022, 272:114994.
[17] Feng D, Feng MQ. Vision-based multipoint displacement measurement for structural health monitoring. *Struct. Control Health Monit.* 2016, 23:876-90.
[18] Liu C, Teng J, Peng Z. Optimal sensor placement for bridge damage detection using deflection influence line. *Smart Struct. Syst.* 2020, 25:169-181.
[19] Dong C-Z, Bas S, Catbas FN. A completely non-contact recognition system for bridge unit influence line using portable cameras and computer vision. *Smart Struct. Syst.* 2019, 24:617-630.
[20] Ge L, Koo KY, Wang M, Brownjohn J, Dan D. Bridge damage detection using precise vision-based displacement influence lines and weigh-in-motion devices: Experimental validation. *Eng. Struct.* 2023, 288:116185.
[21] Chen Z, Yang W, Li J, Yi T, Wu J, *et al*. Bridge influence line identification based on adaptive B-spline basis dictionary and sparse regularization. *Struct. Control Health Monit.* 2019, 26:e2355.
[22] Feng D, Feng MQ. Model updating of railway bridge using *in situ* dynamic displacement measurement under trainloads. *J. Bridge Eng.* 2015, 20:04015019.

[23] Feng D, Feng MQ. Experimental validation of cost-effective vision-based structural health monitoring. *Mech. Syst. Signal Process.* 2017, 88:199-211.
[24] Peng Z, Li J, Hao H. Long-term condition monitoring of cables for in-service cable-stayed bridges using matched vehicle-induced cable tension ratios. *Smart Struct. Syst.* 2022, 29:167-179.
[25] Noble FK. Comparison of OpenCV's feature detectors and feature matchers. *2016 23rd International Conference on Mechatronics and Machine Vision in Practice (M2VIP)*, Nanjing, China, November 28-30, 2016, pp 1-6.
[26] Tan D, Ding Z, Li J, Hao H. Target-free vision-based approach for vibration measurement and damage identification of truss bridges. *Smart Struct. Syst.* 2023, 31:421-436.
[27] Zhan J, Zhang F, Siahkouhi M, Kong X, Xia H. A damage identification method for connections of adjacent box-beam bridges using vehicle–bridge interaction analysis and model updating. *Eng. Struct.* 2021, 228:111551.
[28] Han F, Dan D, Xu Z, Deng Z. A vibration-based approach for damage identification and monitoring of prefabricated beam bridges. *Struct. Health Monit.* 2022, 21:2010-2025.
[29] Jiang C, Xiong W, Wang Z, Cai C, Yang J. Transverse Connectivity and Durability Evaluation of Hollow Slab Bridges Using Surface Damage and Neural Networks: Field Test Investigation. *Appl. Sci.* 2023, 13:4851.
[30] Li S, Wei S, Bao Y, Li H. Condition assessment of cables by pattern recognition of vehicle-induced cable tension ratio. *Eng. Struct.* 2018, 155:1-15.